Originals

Experiments in Fluids 19 (1995) 69–77 © Springer-Verlag 1995

Feasibility study of three-dimensional PIV by correlating images of particles within parallel light sheet planes

M. Raffel, M. Gharib, O. Ronneberger, J. Kompenhans

Abstract One approach to obtain information about the out-of-plane velocity component from PIV recordings is to analyze the height of the peak in the correlation plane. This value depends on the portion of paired particle images, which itself depends on the out-of-plane velocity component and on other parameters. To circumvent problems with other influences (e.g. background light, amount and size of images), images from another light sheet plane parallel to the first one were also captured for peak height normalization. Our experimental results show the feasibility of an out-of-plane velocity estimation by analyzing images of particles within parallel light sheets by spatial cross-correlation.

List of symbols

C	particle density in the flow
d_τ	particle image diameter
f_0, f_1	frames containing images of particles within the first light sheet at $t=t_0$ (frame f_0) and at $t=t_0+\Delta t$ (frame f_1)
f_2	frame containing images of particles within the second light sheet parallel to the first one at $t=t_0+2\Delta t$
F_I	estimator of the loss of image pairs due to in-plane motion
F_O	estimator of the loss of image pairs due to out-plane motion
F_τ	convolution of the particle image intensity distributions
K	factor containing constant parameters in the correlation plane
M	imaging magnification (image size/object size)
n_0	number of particles in the measurement volume at $t=t_0$
$n_{0,1}$	number of particle image pairs in interrogation windows of f_0 and f_1
$n_{1,2}$	number of particle image pairs in interrogation windows of f_1 and f_2
O_z	overlap of the light sheets
$R_C(\underline{s})$	convolution of the mean intensity distributions
$R_D(\underline{s})$	correlation which gives the image displacement
$R_F(\underline{s})$	fluctuating noise component of the cross correlation estimator
$R_{0,1}(\underline{s}_D)$	cross-correlation peak height of interrogation windows of f_0 and f_1
$R_{1,2}(\underline{s}_D)$	cross-correlation peak height of interrogation windows of f_1 and f_2
$\underline{s}$	two-dimensional separation vector in the correlation plane
$\underline{s}_D$	mean particle image displacement in the interrogation cell
t_e	light pulse duration
t_f	frame-transfer time of the video camera
$\underline{u}$	three-dimensional local flow velocity vector (u, v, w)
$\underline{X}_i$	position of the center of an interrogation window in the image plane (2d)
$\underline{x}_i$	position of the center of an interrogation volume in the flow (3d)
(z_2-z_1)	displacement of the light sheets in z-direction
Δt	separation time of the light pulses
Δx_0	x-extension of an interrogation volume
Δy_0	y-extension of an interrogation volume
Δz_0	light sheet thickness

Received: *26 October 1994*/*Accepted*: *22 January 1995*

M. Raffel, O. Ronneberger, J. Kompenhans
DLR, Institut für Strömungsmechanik,
Center for Quantitative Visualisation (CQV)
Bunsenstraße 10, D-37073 Göttingen, Germany

M. Gharib
CALTECH, Graduate Aeronautical Laboratory,
Center for Quantitative Visualisation (CQV)
Pasadena CA 91125, USA

The authors would like to thank DLR for supporting Markus Raffel's and Olaf Ronneberger's visit to Caltech (Center for Quantitative Visualisation), and the Office of Naval Research through the URI grant ONR-URI-N00014-92-J-1610. Dr. Alexander Weigand's generous offer of his experimental set-up and stimulating discussions with Dr. Jerry Westerweel and Dr. Thomas Roesgen are greatly appreciated. Special thanks also to Dr. Christian Willert for his advice regarding the modifications to the DPIV software.

1 Introduction

One limitation for the application of conventional particle image velocimetry (PIV) is its inability to resolve the out-of-plane components of velocity vector fields. Since most of the technologically important flows are three-dimensional, the application of PIV to these flows is rarely conclusive. To overcome the aforementioned shortcomings, a novel idea to estimate the out-of-plane flow component in PIV is described in this paper.

Our approach is based on the quantitative analysis of the location *and height* of the correlation peak. A qualitative analysis of the peak height in conventional DPIV has already been used by Liepmann and Gharib (1992) to define the core boundary of a jet flow. Our aim was to test the concept of relating the behaviour of the correlation function to the motion of the particles normal to two recorded planes in an experiment. This concept is referenced as dual-plane correlation technique or dual-plane PIV in the following.

In its 'classical' form PIV extracts two components of the flow velocity vector by measuring the displacement of tracer particles within a double-pulsed laser light sheet. After the displacement is recorded the knowledge of the time interval Δt between the illumination pulses can be used to obtain the instantaneous velocity vector (Adrian 1991). The particle images resulting from two separate exposures are stored either on the same or on separate recordings (e.g. Willert and Gharib 1991). The velocity vector field is usually determined by subdividing the PIV recording into interrogation windows and employing particle tracking algorithms or statistical evaluation techniques, such as histogram-analysis, analysis of Young's fringes or cross-correlation methods. The statistical methods are widely used as they can be easily implemented into fast, reliable and fully automatic evaluation systems.

Two problems arise when measuring highly three-dimensional flows with PIV. First, it is obvious from the description of the recording process given above that the conventional PIV technique is only applicable to flows within a limited extent of the out-of-plane velocity component. This restriction is imposed because particles moving perpendicular to the light sheet will leave and enter the light sheet in between the two illumination pulses and thus will not correlate when evaluating the PIV recording. This leads to a decreased probability in detecting the particle image displacement, as has been shown by numerical simulations carried out by Keane and Adrian (1990).

Second, allowing a significant velocity component perpendicular to the light sheet plane leads to an additional error because the camera lens reproduces the tracer particles by perspective projection and not by parallel projection. The only way to avoid this error when observing highly three-dimensional flows is to measure all three components of the velocity vectors. It can be shown that measuring only the in-plane components can lead to errors of more than 15% of the mean flow velocity in certain cases (Raffel and Kompenhans, 1994a).

The most commonly used technique to measure instantaneous three-dimensional velocity fields in a plane is stereoscopic PIV. For this technique the achievable accuracy of the measurement of the out-of-plane velocity component is less than that of the in-plane component, but the out-of-plane measurement error can be reduced below 1% of full scale in best cases (Prasad and Adrian 1992). For this purpose specially developed calibration techniques and two recording cameras are necessary. Both cameras need optical access and image shifting devices. That makes the operation of stereoscopic PIV more difficult than that of dual-plane PIV.

2
Mode of operation

2.1
Particle motion through parallel light sheets

A two-dimensional representation of the measurement volume as obtained by a cut perpendicular to the light sheet is given in Fig. 1. To simplify the following explanation an in-plane motion only in x-direction is assumed. The grey area represents particles, which were in the interrogation volume during the first exposure.

When dealing with a sufficient number of particles in the measurement volume, the number of particle image pairs per interrogation cell can be used to estimate the out-of-plane flow component. This number is proportional to n_0, the number of particles within the interrogation volume at t_0 (see Fig. 1a), decreased by the number of second images lost due to out-of-plane motion and by the number lost by in-plane motion (Adrian 1988). Using evaluation methods with a constant size and fixed location of the interrogation window, and assuming a constant particle density C, the number of lost particle image pairs is proportional to the hatched area shown in Fig. 1b.

The number of particles within the measurement volume at location x_0 during the first exposure can be calculated as:

$$n_0 = C \cdot \Delta x_0 \cdot \Delta y_0 \cdot \Delta z_0, \quad \text{with } C = \text{constant}. \tag{1}$$

Two different methods can be used to circumvent the loss of particle image pairs resulting from the in-plane velocity components u and v (Keane and Adrian 1992). This loss of image pairs can be eliminated by using different sizes of interrogation windows and therefore of the interrogation volumes in x- and y-direction Δx_0, Δy_0 and Δx_1, Δy_1 and identical locations of their centers $\underline{x}_1 = \underline{x}_0$ (see Fig. 2a). It is also possible to use an identical size of interrogation volumes centered at $\underline{x}_0$ and $\underline{x}_1$ (see Fig. 2b). In the latter case, the centers

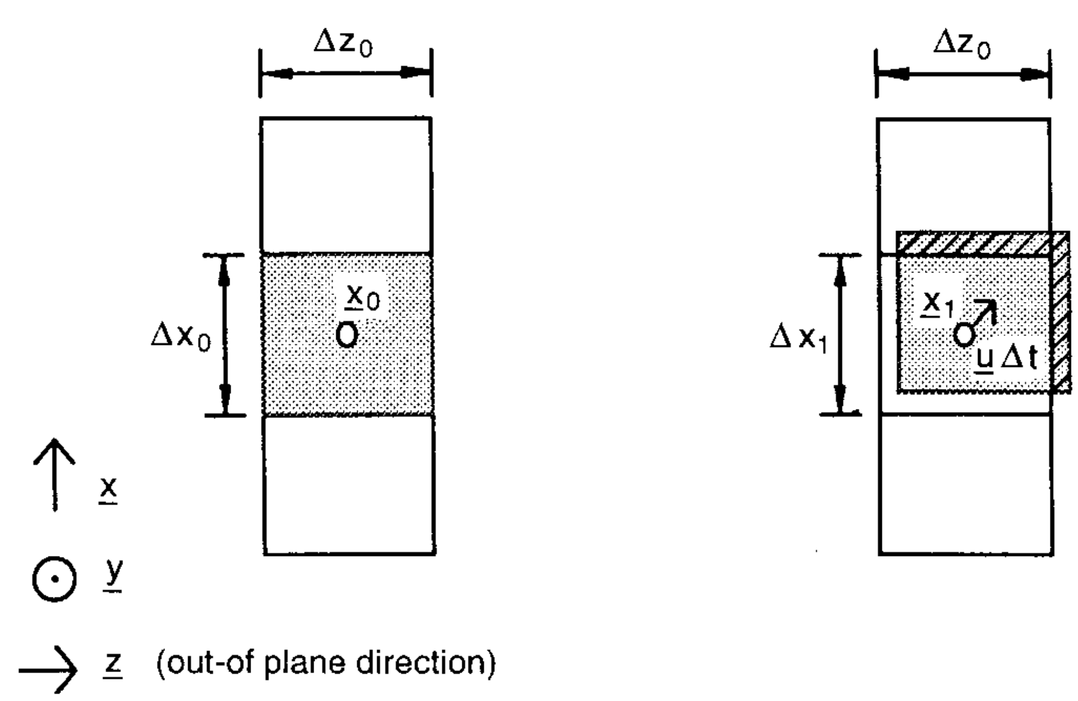

Fig. 1a, b. Sketch of particles moving through a light sheet (main extension in x- and y-direction) at two different times. **a** $t = t_0$; **b** $t = t_0 + \Delta t$

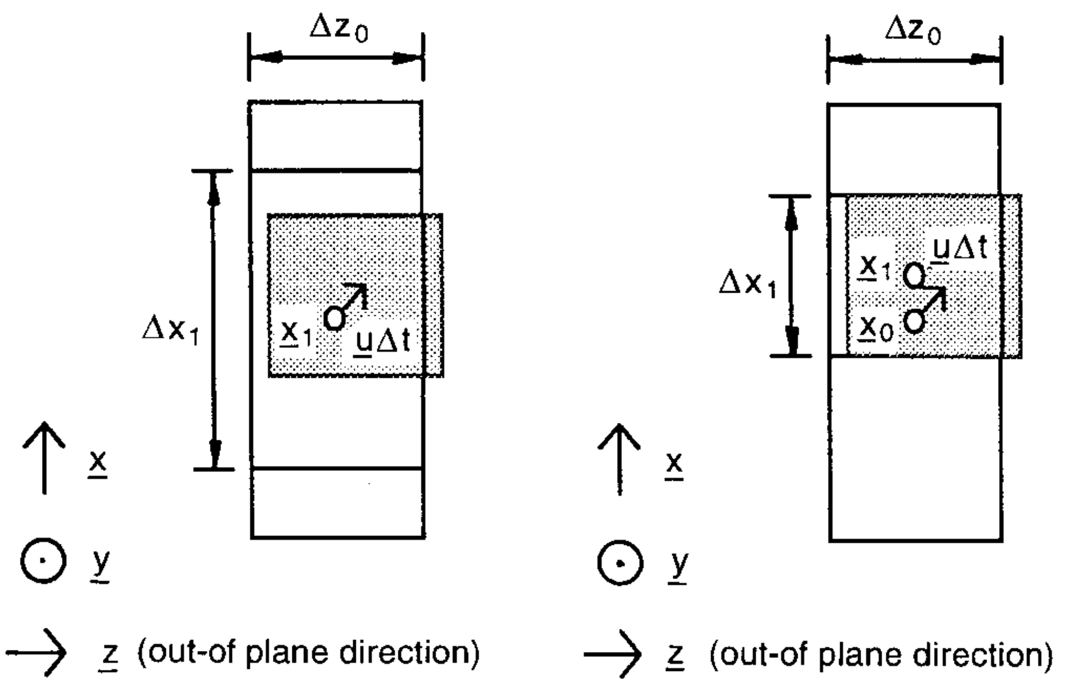

Fig. 2a, b. Size and location of the interrogation volume and position of the particles, which were illuminated by the first light pulse, represented at the time of the second exposure. **a** method of enlarged interrogation window at $t = t_0 + \Delta t$; **b** method of adapted interrogation window position at $t = t_0 + \Delta t$

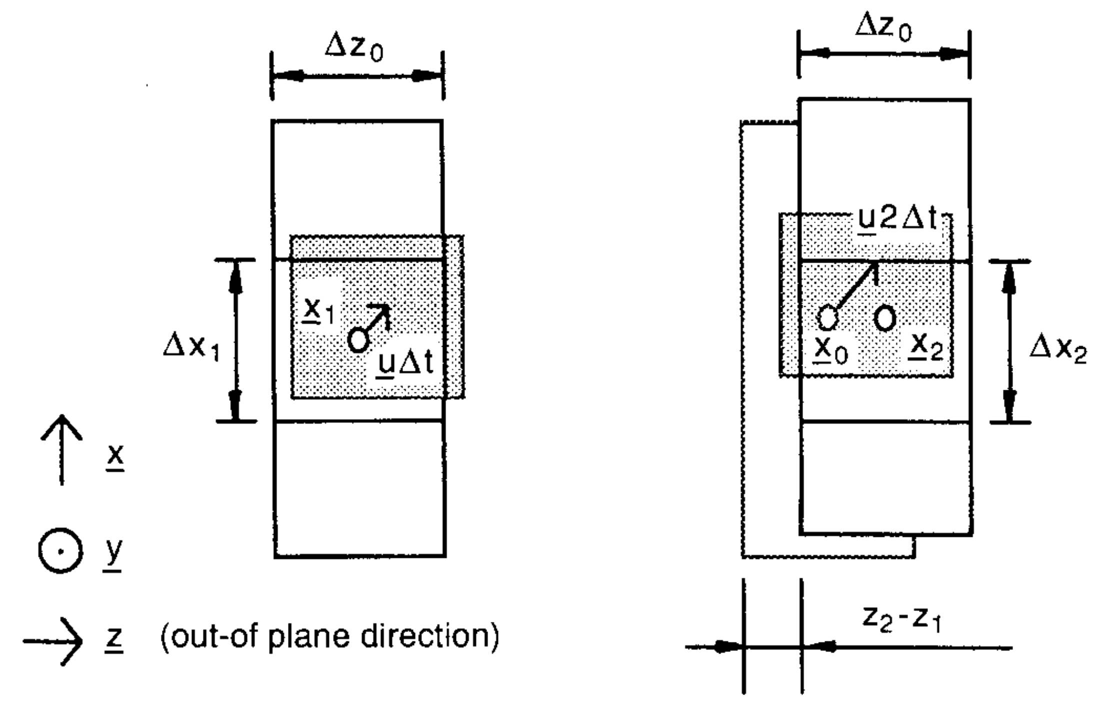

Fig. 3a, b. Size and location of the interrogation volume and position of the particles, which were illuminated by the first light pulse, represented at the time of the second exposure (a) and third exposure (b). **a** $t = t_0 + \Delta t$; **b** $t = t_0 + 2\Delta t$

of the interrogation windows have to be displaced by the mean particle image displacement of the observed area.

For a later improvement of the technique, either method and their combinations can be used to reduce the loss of particle image pairs to the fraction caused by the out-of-plane velocity component w. However, the dual-plane correlation technique worked well even in case of a certain in-plane pair loss, since, beside others, also their influence is minimized by the procedure described in the following.

During the experiments, we first captured images of tracer particles within a single light sheet plane on two separate frames f_0 and f_1 (see Fig. 3a). The time separation between both exposures is denoted by Δt. In addition, after a delay of Δt, images of tracer particles, illuminated by a second light sheet parallel to the first one, were captured on a third frame f_2 (see Fig. 3b). The second light sheet was displaced in the direction of the largest out-of-plane components by a distance of $(z_2 - z_1)$. This distance was chosen to be smaller than the light sheet thickness Δz_0. This resulted in an overlap $O_z = 1 - (z_2 - z_1)/\Delta z_0$ between the two light sheets in z-direction.

The recording and evaluation of a third frame of particles within a parallel light sheet has the following advantages: (1) the influence of the loss of image pairs due to the in-plane velocity components can be reduced; (2) the ambiguity of the sign of the out-of-plane velocity component can be removed; (3) a larger out-of-plane velocity component can be tolerated; and (4) a better signal-to-noise ratio can be achieved. This becomes clear when analysing the number of matched particle images, which can be detected within the separate recordings, as explained below.

Assuming that the out-of plane particle motion $w\Delta t$ is positive and always smaller than the light sheet thickness Δz_0, and that the intensity distribution in the light sheet is constant in z-direction, the number of matched particle images, which can be detected within the separate recordings (f_0 and f_1) can be calculated as:

$$n_{0,1} = C \cdot (\Delta x - |u\Delta t|) \cdot (\Delta y - |v\Delta t|) \cdot (\Delta z_0 - w\Delta t),$$

$$\text{if } 0 \leqslant w\Delta t \leqslant \Delta z_0. \tag{2}$$

Within the limits given below, the number of particle image pairs within the interrogation windows of separate recordings of the second and third exposure f_1 and f_2 can be calculated as:

$$n_{1,2} = C \cdot (\Delta x - |u\Delta t|) \cdot (\Delta y - |v\Delta t|) \cdot (O_z \Delta z_0 + w\Delta t),$$

$$\text{if } -O_z \Delta z_0 \leqslant w\Delta t \leqslant (z_2 - z_1). \tag{3}$$

Combining Eqs. (2) and (3), the following formula for the estimation of the out-of-plane velocity component can be obtained:

$$w = \frac{\Delta z_0}{\Delta t} \frac{n_{1,2} - O_z n_{0,1}}{n_{1,2} + n_{0,1}}, \quad \text{if } 0 \leqslant w\Delta t \leqslant (z_2 - z_1). \tag{4}$$

It must be mentioned that the Eqs. (1), (2) and (3) can be combined in different ways. Furthermore, it must be kept in mind, that the exact numbers for $n_{0,1}$ and $n_{1,2}$ cannot be calculated. They can only be estimated with a certain error. We decided to use the combination yielding Eq. (4) for our evaluation. This decision was based on the assumption that the main sources of errors can be modeled as factors contained in the calculated estimators. Identical factors contained in the estimation of $n_{0,1}$ and $n_{1,2}$ are eliminated when using Eq. (4). The error sources contained in the estimators are described in the following section.

2.2
Estimation of particle image pair frequency by spatial cross correlation

In this section, the estimation of the frequency of particle image pairs by spatial cross-correlation is described. Therefore the theory and notation developed by Adrian (1988) and by Keane and Adrian (1990, 1992) will be used. According to them it is convenient to decompose the estimator for cross-correlation of single-exposure frames into three components. Each of them is a function of the two dimensional separation vectors $\underline{s}$ in the correlation plane:

$$R(\underline{s}) = R_c(\underline{s}) + R_D(\underline{s}) + R_F(\underline{s}).$$

The influences considered by this decomposition are the convolution of the mean intensity distributions $R_C(\underline{s})$, the fluctuating noise component $R_F(\underline{s})$ (generated by images of distinct particles) and the correlation peak giving the image displacement $R_D(\underline{s})$ of identical particles. The basis of the evaluation procedure we used is the fact that the strength of the displacement peak $R_D(\underline{s})$ is proportional to the number of image pairs in the correlation windows. The assumption of a sufficiently low variance of the velocity within each interrogation cell leads to the following simplified model:

$$R_D(\underline{s}) = F_I(\underline{s}_D, \underline{X}_i, \underline{X}_{i+1}, \Delta x, \Delta y) \cdot F_O(w\Delta t, z_{i+1} - z_i, \Delta z_0) \cdot F_\tau(\underline{s} - \underline{s}_D) \cdot K.$$

$F_I(\underline{s}_D, \underline{X}_i, \underline{X}_{i+1}, \Delta x, \Delta y)$ describes the decrease by the fraction of second images lost by in-plane motion as a function of the particle image displacement $\underline{s}_D$, the size of the interrogation windows and therefore of $\Delta x, \Delta y$, and the location of both interrogation windows $\underline{X}_i, \underline{X}_{i+1}$. The influence of the fraction of second images lost by out-of-plane motion is considered by $F_O(w\Delta t, z_{i+1} - z_i, \Delta z_0)$ which is a function of the out-of-plane particle displacement $w\Delta t$ and the shift of the light sheets in z-direction $z_{i+1} - z_i$ and their thickness Δz_0. The assumption of a constant intensity distribution of the light sheets in z-direction yields: $F_{O;0,1}(w\Delta t, \Delta z_0) = 1 - \frac{w\Delta t}{\Delta z_0}$ for the case of the same light sheet location, and $F_{O;1,2}(w\Delta t, \Delta z_0, z_2 - z_1) = O_z + \frac{w\Delta t}{\Delta z_0}$ for the case of different light sheet locations. $F_\tau(\underline{s} - \underline{s}_D)$ is the convolution of the particle image intensity distributions. The effects of other parameters on the displacement peak are combined together in K.

In order to use the height of the correlation peak $R(\underline{s}_D)$ as an indicator for the loss of particle image pairs due to out-of-plane motion, the influence of other parameters has to be reduced. To eliminate the convolution $R_C(\underline{s})$, the mean intensities can be subtracted in each interrogation window. The fluctuating noise $R_F(\underline{s})$ is a source of error, which cannot be reduced easily. A problem arises after computing the correlation of images of tracer particles within the same light sheet $R_{0,1}(\underline{s})$ and within different light sheets $R_{1,2}(\underline{s})$. The peak position found in two different correlation planes might not be the same. The location $\underline{s}_D$ for the comparison of the peak heights has to be determined by analyzing the correlation plane $R_{i,i+1}(\underline{s})$, which has the better signal-to-noise ratio. That ensures that not the maximum of the fluctuating noise $R_{F,\max}$, which may be found by the peak finding algorithm in the correlation plane of lower signal-to-noise ratio, was used.

The effects of other parameters can be reduced as follows: $R_D(\underline{s})$ has to be normalized by the square root of the product of the autocorrelation peaks of both interrogation windows. In order to minimize the loss of particle image pairs due to in-plane motion, the window positions or sizes can be adapted as described in the previous section. In the presence of strong velocity gradients the peak strength should be analyzed using the peak volume. This can be done either by computing the sum of all grey values contained in the peak or by analyzing a fitted profile when dealing with low resolution PIV.

In our feasibility study we estimated the out-of-plane velocity component by using the correlation peak height of images of tracer particles in the same light sheet $R_{0,1}(\underline{s}_D)$ and of images of tracer particles in different light sheets $R_{1,2}(\underline{s}_D)$ to approximate $\frac{n_{0,1}}{n_0}$ and $\frac{n_{1,2}}{n_0}$:

$$w = \frac{\Delta z_0}{\Delta t} \frac{R_{1,2}(\underline{s}_D) - O_z R_{0,1}(\underline{s}_D)}{R_{1,2}(\underline{s}_D) + R_{0,1}(\underline{s}_D)}, \quad \text{if } 0 \leqslant w\Delta t \leqslant (z_2 - z_1). \tag{5}$$

We eliminated two of the above-mentioned effects by subtracting the mean intensity of the interrogation window and by normalizing the correlation peak height with the square root of the product of the autocorrelation peaks. Therefore, the following simplifications are implied in formula (5):

(1) A top-hat intensity profile of the light sheets in z-direction has been assumed instead of a Gaussian distribution. This leads to the fact that $F_O(w\Delta t, z_{i+1} - z_i, \Delta z_0)$, which is the normalized correlation of the intensity distributions in z-direction of two successive pulsed light sheets and is therefore also a Gaussian function, is approximated by a triangle function. (2) The effect of the variation of the displacement within the interrogated cell, and the fraction of second images lost by in-plane motion $F_I(\underline{s}_D, \underline{X}_i, \underline{X}_{i+1}, \Delta x, \Delta y)$ is assumed to be identical for both correlations. This is only a rough approximation as long as the frames f_1 and f_2 are not captured at the same time. (3) The fluctuating noise component $R_F(\underline{s})$ is neglected. Its effect on the measurement accuracy can be reduced by averaging results over neighboring interrogation cells. However, this has to be balanced against a decrease in spatial resolution.

3
Result of a simple numerical simulation

To obtain a first impression of the properties of the velocity estimation given in equation (5) we performed a simple numerical simulation assuming a Gaussian intensity distribution of the particle images on a noise-free background. The locations of particle images in three frames f_0, f_1 and f_2 were computed based on a random distribution of particles moving with a varying velocity $u = (0, 0, w = (x/x_{\max})(1 - O_z)\Delta z_0/\Delta t)$. The z-component of the particle displacement is shown as a line in Fig. 4. It varies from $z = 0$ up to $z = 3.15$ mm at $x = x_{\max}$. In correspondence to our experimental investigations the overlap of the light sheets at $t = t_0 + \Delta t$ and $t = t_0 + 2\Delta t$ was set to $O_z = 17\%$ of the light sheet thickness ($\Delta z_0 = 3.75$ mm in this case). Each dot in Fig. 4 represents a grid point of the velocity field obtained by our method. The averages of the estimated velocity values show linear behavior.

As mentioned in Sect. 2.1, Eq. 5, which was used for evaluation, compensates for sources of errors, which can be modeled as factors contained in the calculated estimators. A more detailed error analysis can show that errors, which can be described by summands contained in the cross-correlation estimator $R(\underline{s})$ such as fluctuating noise component $R_F(\underline{s})$, influences the result especially at the boundary of the measurement area (see Fig. 4).

4
Experimental setup

In our experiments we observed particles in a vortex ring flow using a frame-transfer CCD-video camera and the standard

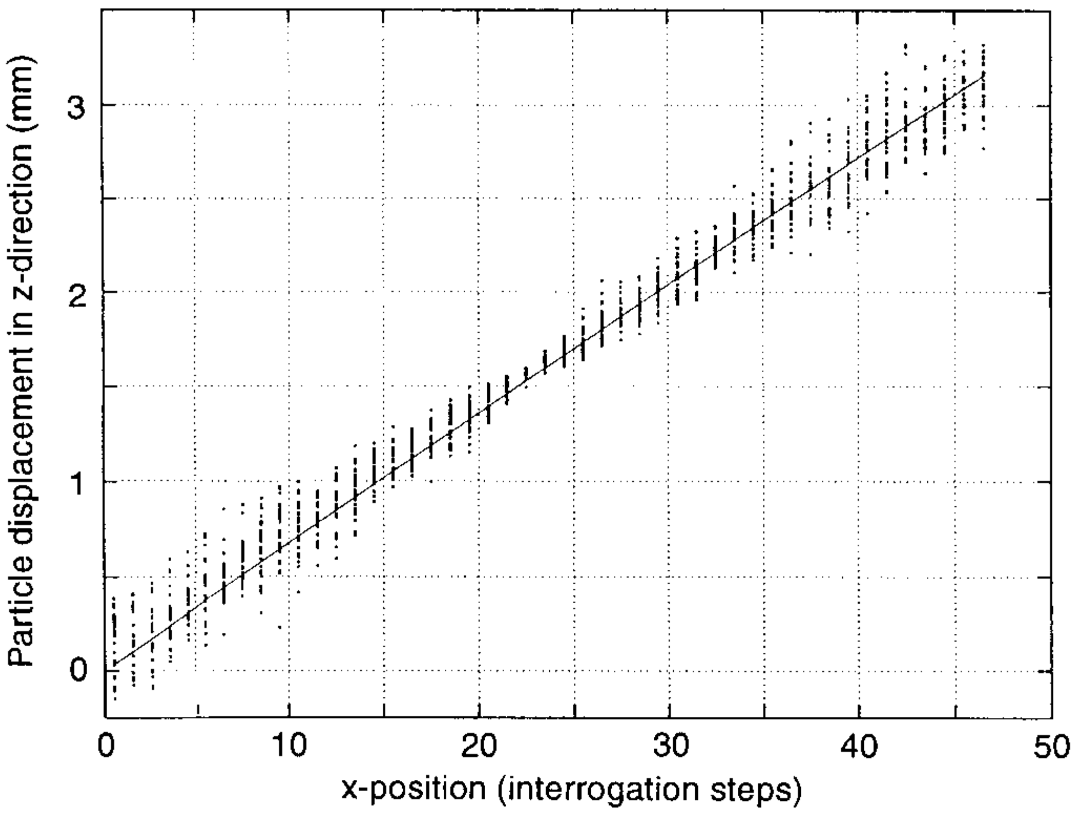

Fig. 4. Evaluation of computer generated images

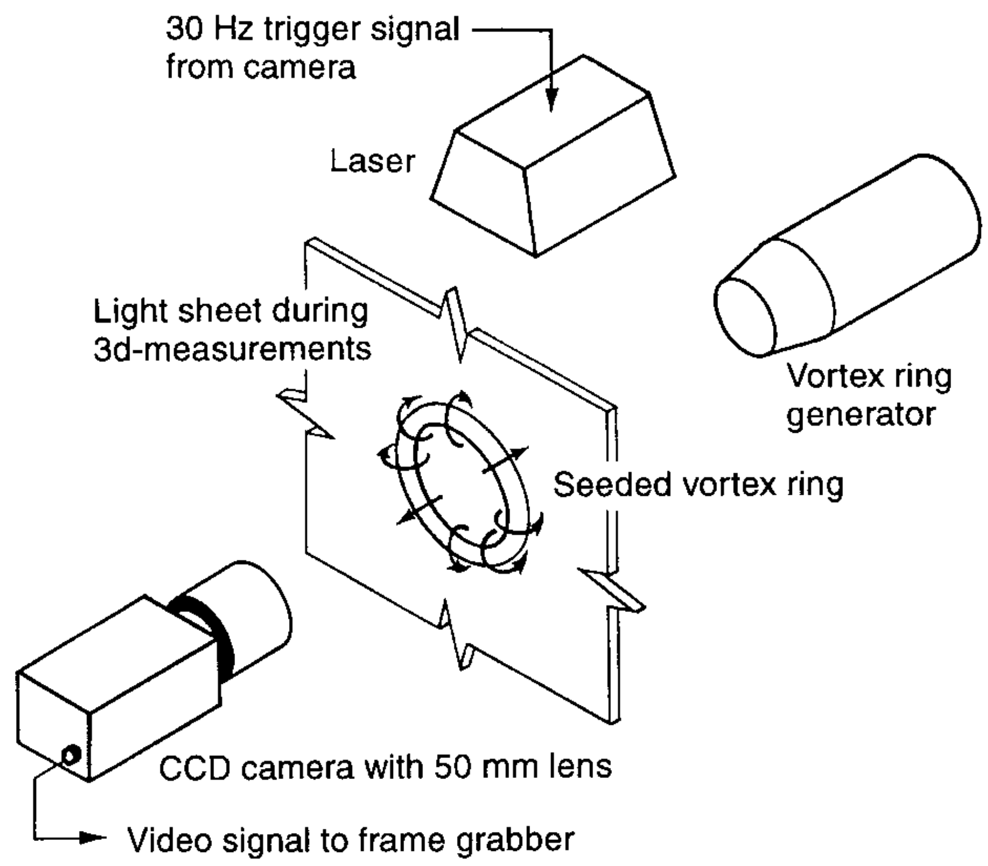

Fig. 5. Sketch of the main components of the setup

DPIV equipment developed by the research group of Prof. Mory Gharib. Glass-spheres with a diameter of 10 μm were mixed with water in a plexiglas tank. The vortex rings were generated by a 30 mm piston that pushes water out of a sharp-edged cylindrical nozzle into the surrounding fluid. The piston was driven by a linear traversing mechanism and a computer controlled stepper motor. A detailed description is given by Weigand (1993).

The flow generated by this setup is well suited for three-dimensional measurements since its properties are documented and tested during various previous experiments (Weigand and Gharib 1994). The vortex ring experiment offers a good challenge for the presented measurement technique, since the obtained flow field is sufficiently complex and reproduces reasonably. The setup was already used for three-dimensional particle imaging using a single camera by Willert and Gharib (1992).

Figure 5 shows the main components of the setup except the light sheet shaping optics and the electronic equipment. The arrangement of the optical and the electro-mechanical components are shown in Fig. 6 and are described below.

An argon-ion laser produced a continuous beam of about 6 Watt output power. An electromechanical shutter controlled by the DPIV timer box generated light pulses with a pulse length of $t_e = 5$ ms and a pulse separation time of $\Delta t = 33$ ms. The shutter was phase locked with the video camera which had a frame-transfer time of $t_f = 2$ ms. The aperture of the shutter was of a size that cuts off the outer area of the laser beam of lower intensity. A computer controlled micro stepper motor with a mirror mounted to one end of the shaft was used as a scanner, which, together with the cylindrical scanner lens (see Fig. 6), generated a parallel displacement of the light sheet. An additional cylindrical lens in front of the scanner mirror focused the light onto the mirror and thus compensated for the confluencing effect of the scanner lens onto the beam. The light sheet shaping lens had a focal length small enough to generate a light sheet height that was twice as large as the height of the observation field. As a result, the variation of the light intensity was held small with respect to the observed field.

The scanner was phased locked to the video signal of the recording camera and alternated the light sheet location after

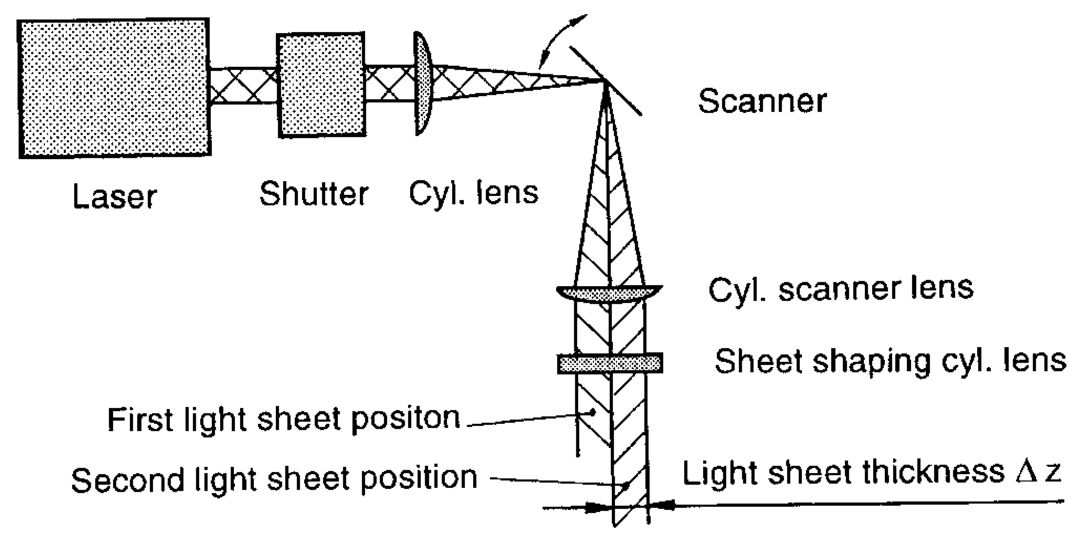

Fig. 6. Sketch of the optical components

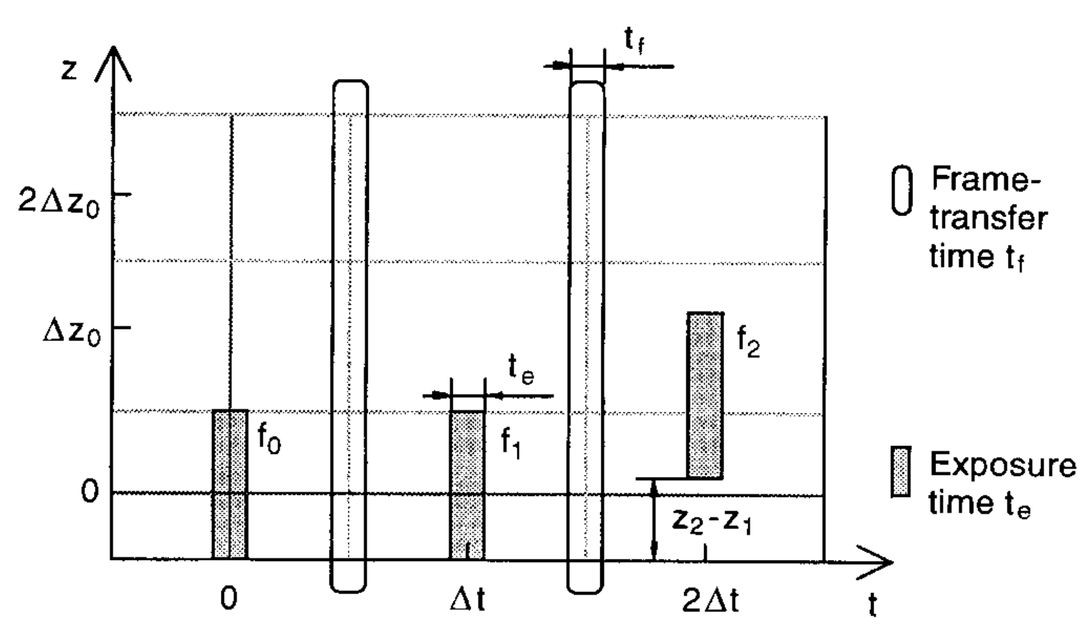

Fig. 7. Timing diagram of image capture and light sheet position

each second capture of a complete video frame (see Fig. 7). Synchronized with the motion of the piston three subsequent video frames were captured. Two frames contain images of tracer particles within the same light sheet orientated perpendicular to the vortex ring axis (f_0 and f_1 captured at $t = t_0$ and $t = t_0 + \Delta t$ respectively). The third frame contains images of tracer particles within a light sheet parallel to the first one (f_2 captured at $t = t_0 + 2\Delta t$). The shift of the light sheet was $(z_2 - z_1) = 2.5$ mm resulting in an overlap of $O_z = 17\%$ of the light sheet thickness ($\Delta z_0 = 3$ mm).

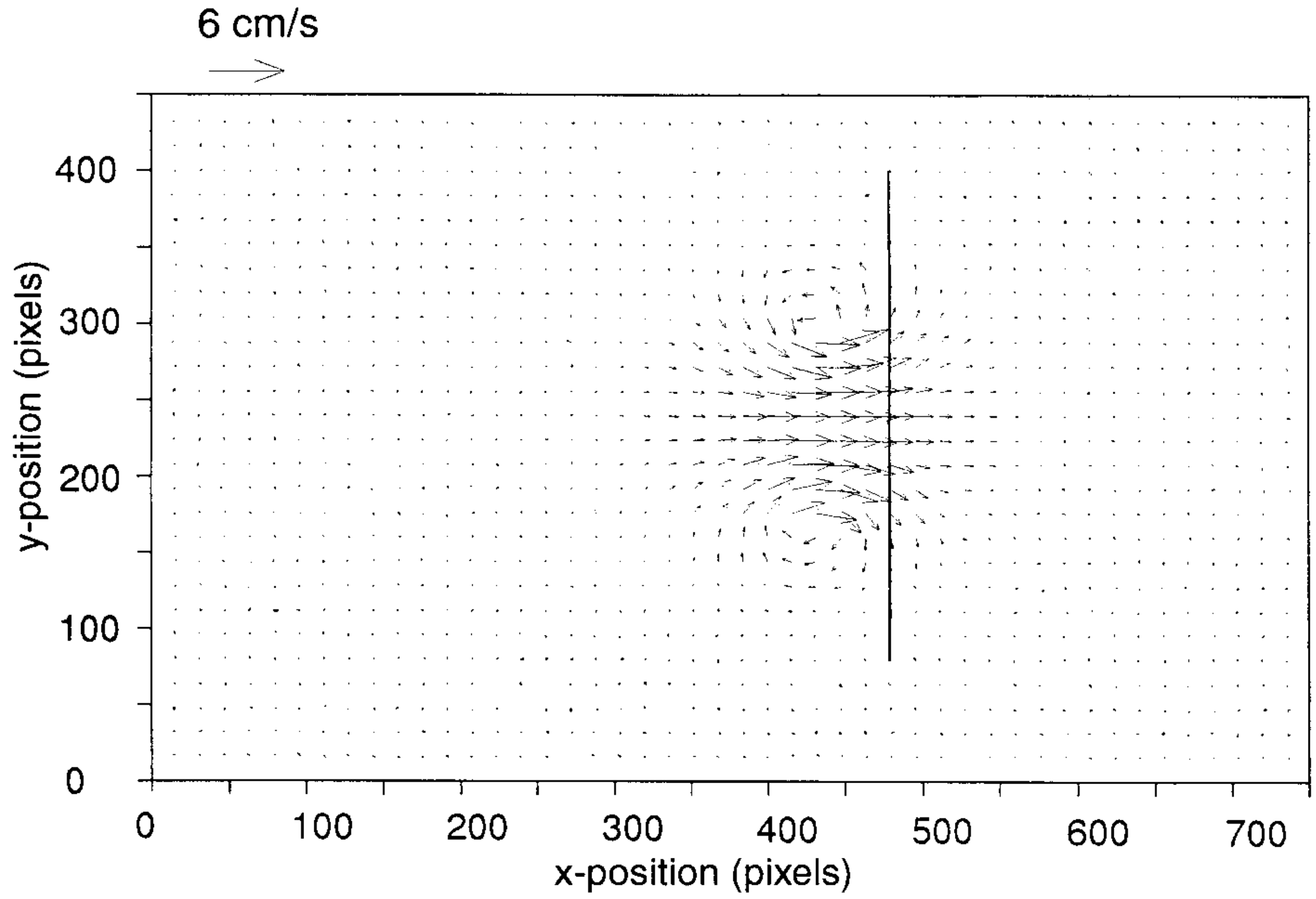

Fig. 8. Flow field in an intersection on the vortex ring axis

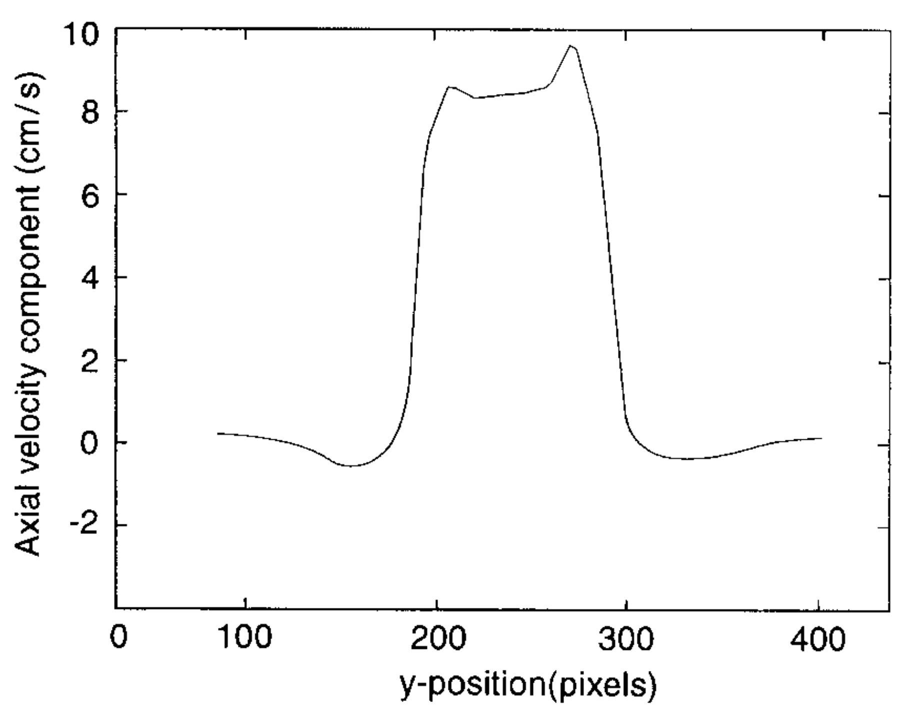

Fig. 9. Velocity component parallel to the vortex ring axis along the line shown in Fig. 8

5 Experimental results

To obtain more information about the flow field generated by the setup described above we first took PIV-data along the centerline of the vortex ring (Fig. 8).

The axial components of the velocity vectors along the indicated line give information on the out-of-plane velocity component we had to expect when observing the flow field in a plane perpendicular to the vortex ring axis. The magnitude of this velocity component parallel to the axis is plotted in Fig. 9.

Following the described method, we then captured images of particles within two parallel light sheets onto three different frames. Both light sheet planes were orientated perpendicular to the vortex ring axis as shown in Fig. 5. The frames were evaluated by correlating f_0 with f_1 and f_1 with f_2, detecting the location of the stronger peak, and storing the normalized intensities of both correlation planes at this location for each

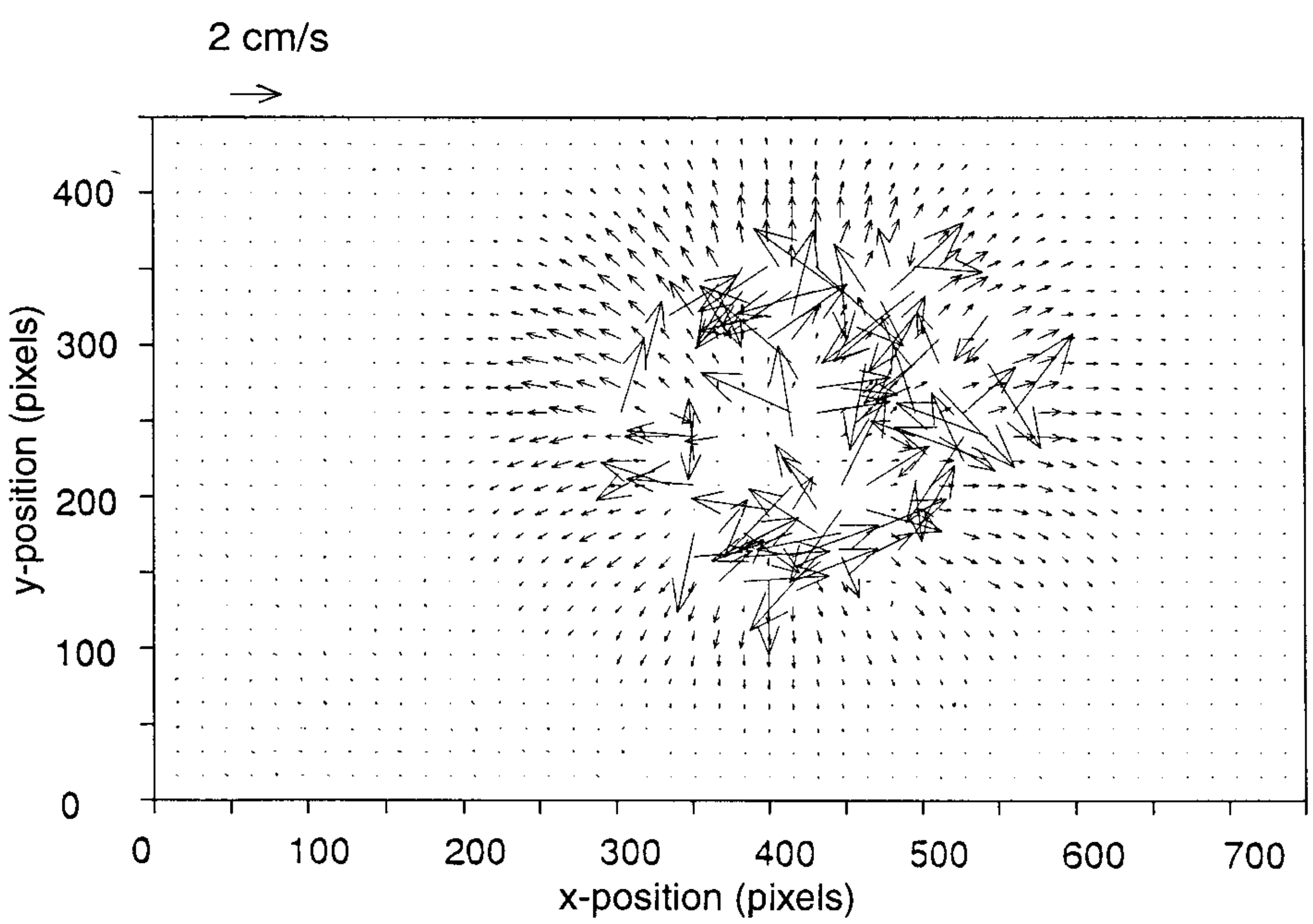

Fig. 10. Velocity vector map obtained by images of particles illuminated by the same light sheet

interrogation cell. The size of the interrogation windows was 32×32 pixels and the interrogation stepwidth in both the x- and y-direction was 16 pixels. The results of the evaluation of the frames f_0 and f_1 containing images of particles within the same light sheet show outliers in a ring near the center of the flow field (see Fig. 10). This area of low detection probability is caused by the decreased seeding density near the center of the vortex ring and by the strong out of plane motion in the center of the observed field.

The heights of the tallest peaks in the cross correlation planes $R_{0,1}(s_D)$ are shown in Fig. 11. They clearly show the influence of the out-of-plane velocity component (i.e. low correlation peak heights in the center of the vortex ring).

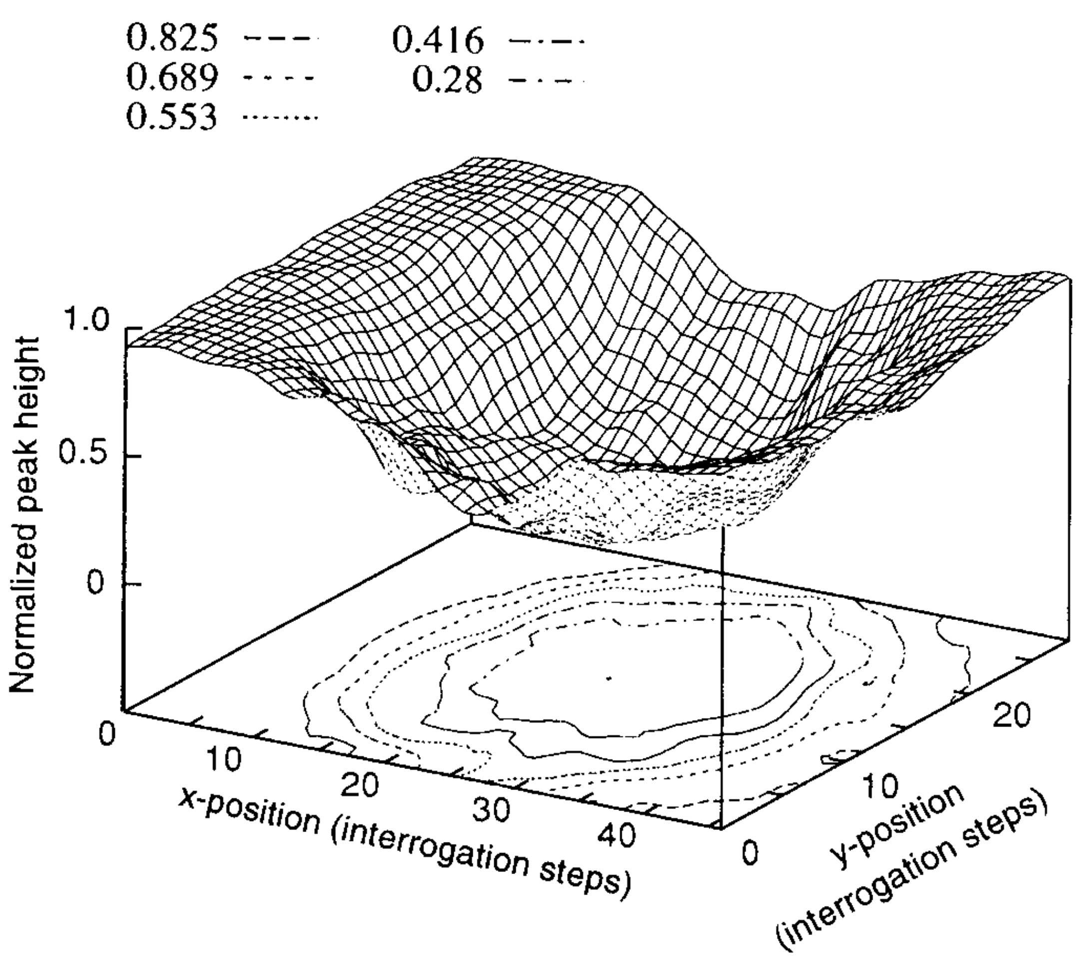

Fig. 11. Cross correlation peak heights of images of particles illuminated by the same light sheet (smoothed by a spatial averaging (3×3 kernel) for this representation)

The results of the evaluation of the frames f_1 and f_2 show outliers in a ring further outward (see Fig. 12). The values of the heights of the correlation peaks $R_{1,2}(\underline{s}_D)$ are shown in Fig. 13. In this case out-of-plane velocity components increase the correlation peak heights.

The following evaluation procedure was used to take advantage of the images captured in different planes. The intensity distributions $R_{0,1}(\underline{s})$ of the correlations of the frames f_0 and f_1 and the intensity distributions $R_{1,2}(\underline{s})$ of the correlations of frames f_1 and f_2 were computed and normalized. The distribution containing the highest peak of the interrogated cell was then used to determine the particle image displacement estimator $\underline{s}_D$. This procedure reduces the number of outliers (see Fig. 14) and therefore shows that compared to conventional PIV a larger out-of-plane component can be tolerated. The peak positions found by this procedure were used to find the correct and identical locations in both cross correlation planes for intensity analysis. Figure 15 shows the plot of the out-of-plane velocity distribution computed from the intensities found in the procedure described above and according to Eq. (5). In contrast to the results obtained by evaluating only two frames (see Fig. 11 and Fig. 13) the expected structures of the flow can now be seen in Fig. 15. Errors arising from the perspective projection were not accounted for, because the out-of-plane velocity component of this specific flow field is approximately zero at the edges of the observation field where the influence of the perspective projection becomes important.

The maximum value of the out-of-plane velocity obtained by the dual-plane correlation technique, of 2.9 mm/33 ms = 8.79 cm/s is in good correspondence with the maximum shown in Fig. 9. Minimum values of the measured velocity distribution are approximately zero in both cases.

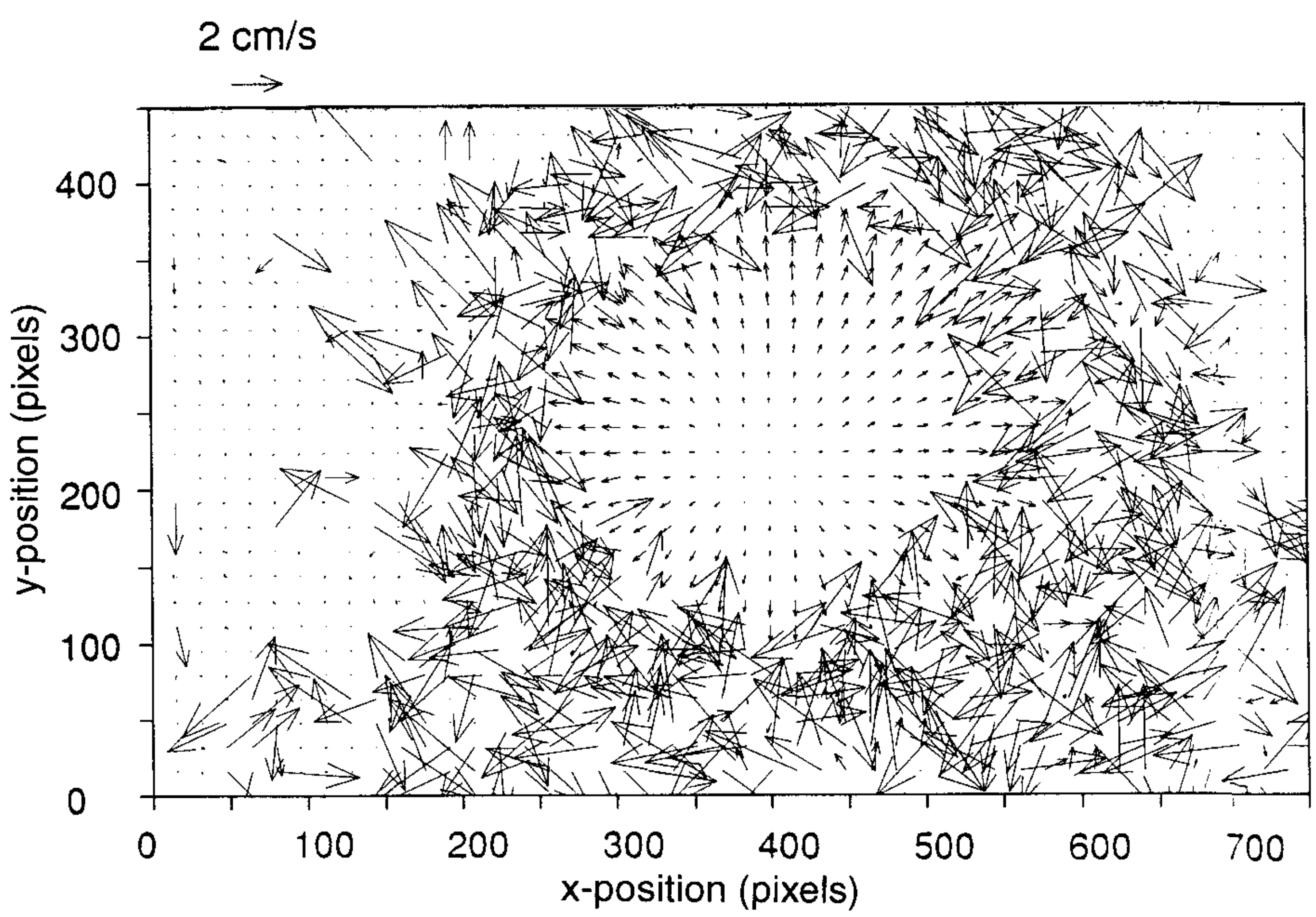

Fig. 12. Velocity vector map obtained by images of particles illuminated by different light sheets

The final result is shown in Fig. 16 in a three-dimensional representation.

6
Conclusions

In this study, we demonstrated the feasibility of using information rendered by the correlation function to estimate the out-of-plane components of velocity fields. Among other limitations, a larger number of particle images per interrogation window is required for the described dual-plane correlation technique than for conventional PIV. This becomes clear if considering that a single particle image pair gives only binary information into which of the two light sheets the particle moved. The existence of a practically achievable maximum of the image density therefore results in a lower spatial resolution and/or accuracy compared to the in-plane easurement. Furthermore, the limits of the equations given in Sect. 2 show that our first approach to this technique is only applicable to flows with out-of-plane components in one direction. However, the results of this approach and the ease of operation of the described technique are encouraging.

In future investigations the influence of parameters like the intensity distribution of the light sheet in z-direction, the velocity gradients and the loss-of-pairs due to in-plane motion should be regarded to increase the resolution of the measurement. In contrast to stereoscopic PIV the out-of-plane measurement error of dual-plane PIV can not easily be estimated by analyzing the in-plane measurement error.

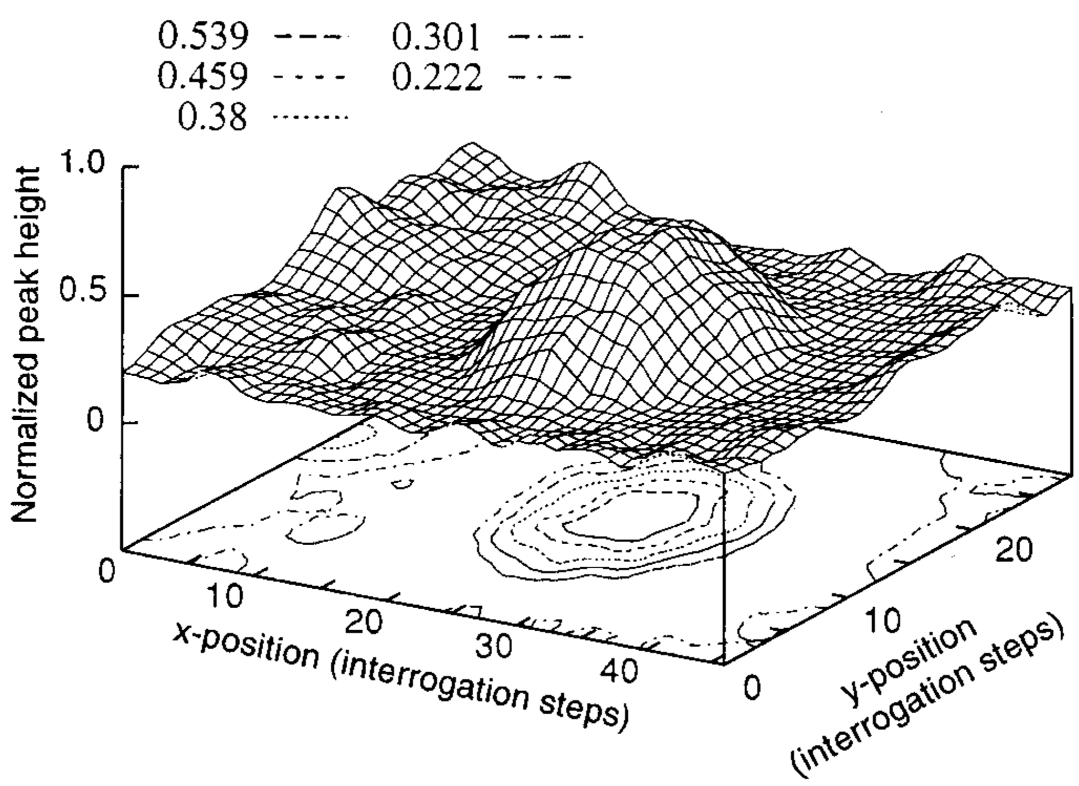

Fig. 13. Correlation peak heights of images of particles illuminated by different light sheets (smoothed by a spatial averaging (3 × 3 kernel) for this representation)

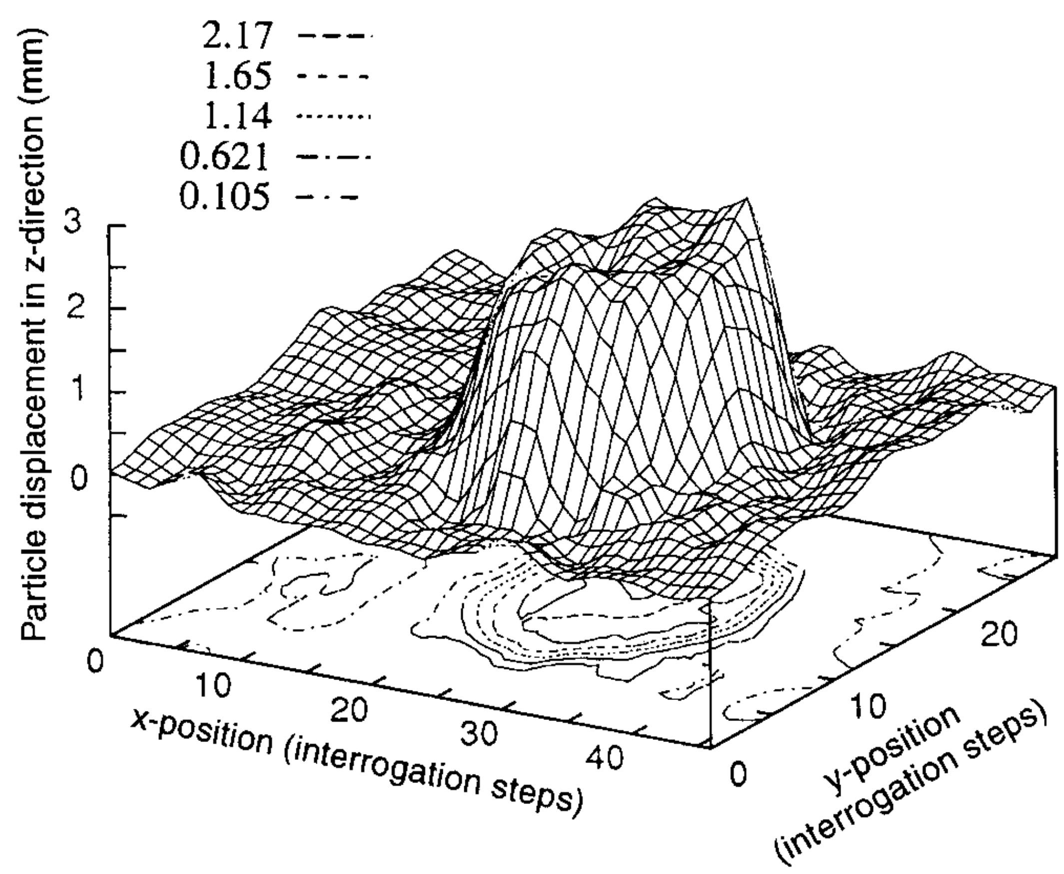

Fig. 15. Out-of-plane velocity distribution obtained by analysing the results of the correlation peaks $R_{0,1}(S_D)$ and $R_{1,2}(s_D)$ for each interrogation cell (smoothed by a spatial averaging (3 × 3 kernel) for this representation)

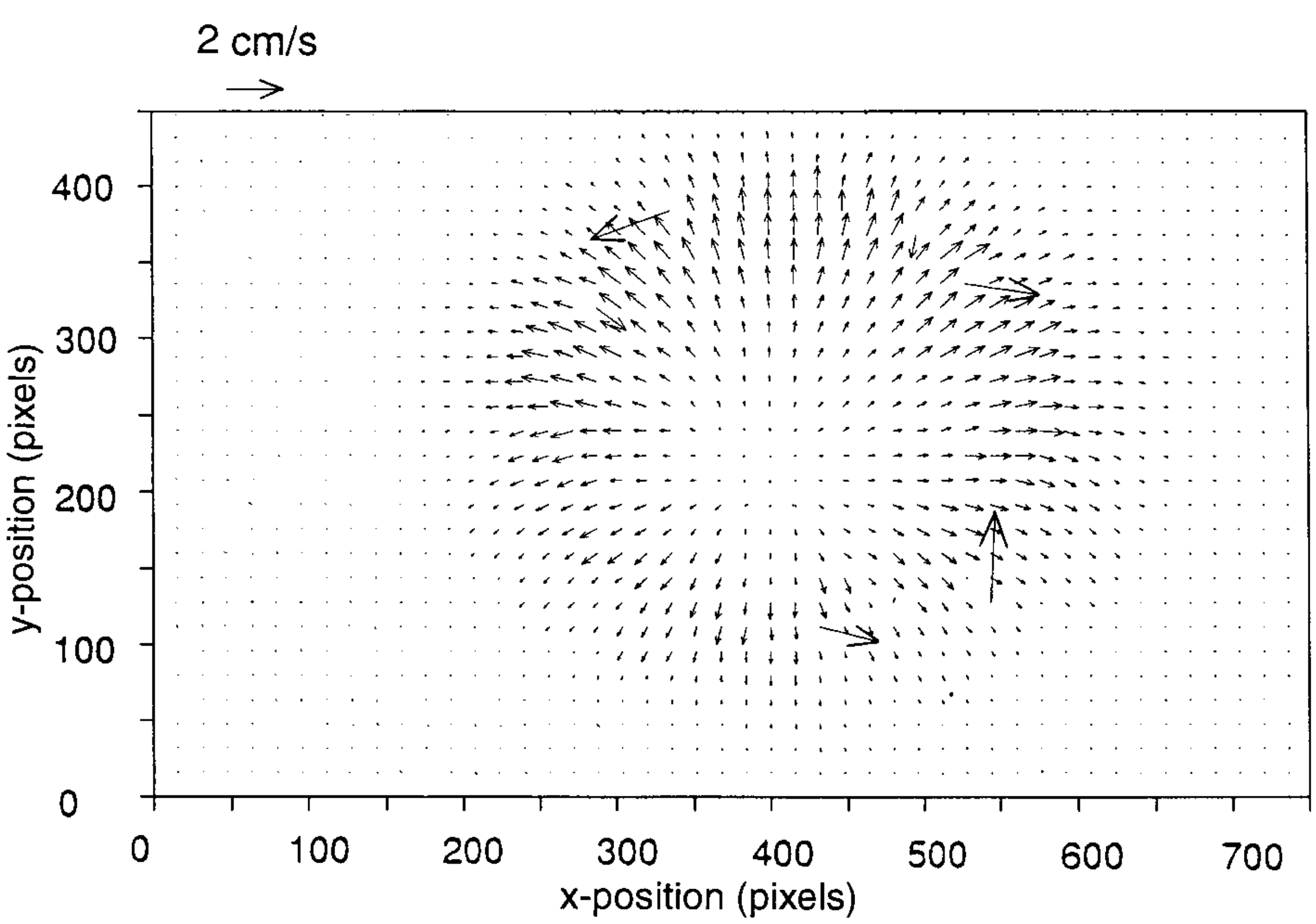

Fig. 14. In-plane velocity vector map obtained by considering the strongest peak of both correlations $R_{0,1}(s)$ and $R_{1,2}(s)$ for each interrogation cell

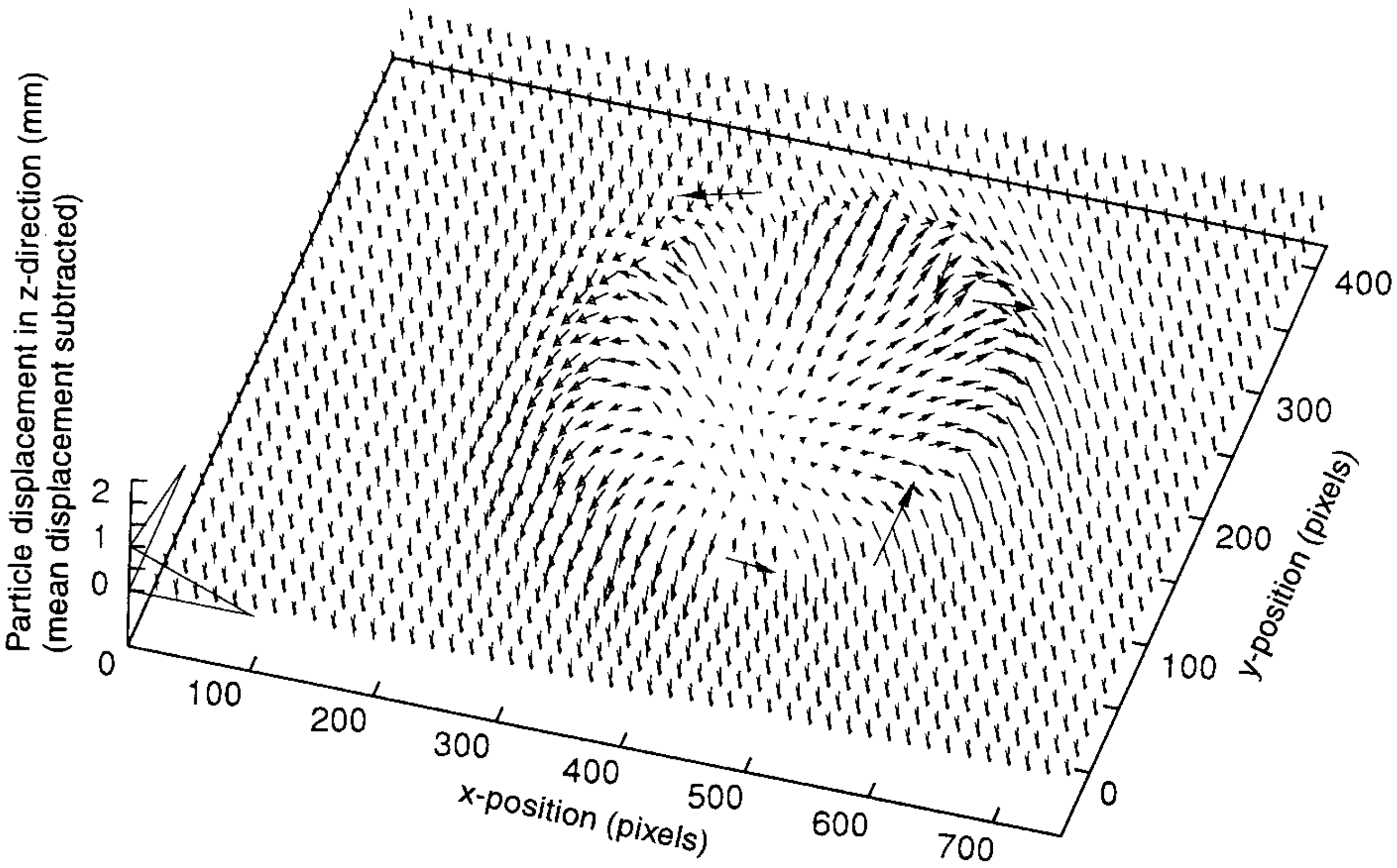

Fig. 16. Three-dimensional representation of the velocity vectors of the observed plane (raw data without any smoothing, data validation or interpolation)

Further work is required to improve and verify the accuracy of the technique. High speed video cameras already used for PIV in high speed flows (Raffel et al. 1994b), and multiple oscillator pulse lasers enable to capture images of particles in two different light sheets quasi-simultaneously. The recording of a fourth frame would allow to detect out-of-plane particle motion in positive and negative direction. The operation of dual-plane PIV is easier than that of stereoscopic PIV, since the only calibration necessary is the determination of thickness and overlap of the light sheets. Furthermore, only one camera is needed.

However, even if the accuracy of the technique presented here could not be increased, it reduces the number of outliers and can be used for an out-of-plane velocity estimation, which increases the accuracy of the in-plane measurement considerably by minimizing the measurement error caused by the perspective projection of the out-of-plane velocity component.

Reference

Adrian RJ (1988) Statistical properties of particle image velocimetry measurements in turbulent flows. In: Laser Anemometry in Fluid Mechanics III (ed. RJ Adrian, T Asanuma, DFG Durao, F Durst and JH Whitelaw): 115–129

Adrian RJ (1991) Particle-imaging techniques for experimental fluid mechanics. Ann Rev Fluid Mech 23: 261–304

Keane RD; Adrian RJ (1990) Optimization of particle image velocimeters. Part I: Double pulsed systems. Meas Sci Technol 1: 1202–1215

Keane RD; Adrian RJ (1992) Theory of cross-correlation analysis of PIV images. Appl Sci Res 49: 191–215

Liepmann D; Gharib M. (1992) The role of streamwise vorticity in the near field entrainment of round jets. J Fluid Mech 245: 643–668

Prasad AK; Adrian RJ (1992) Stereoscopic particle image velocimetry applied to liquid flows. 6 Int Symp on Appl of Laser Techniques to Fluid Mechanics, Lisbon, Portugal, paper 6-1

Raffel M; Kompenhans J (1994a) Error analysis for PIV recording utilizing image shifting. 7 Int Symp on Appl of Laser Techniques to Fluid Mechanics, Lisbon, Portugal, paper 35-5

Raffel M; Kompenhans J; Stasicki B; Bretthauer B; Meier GEA (1994b) Velocity measurement of compressible air flows utilizing a high-speed video camera. Exp Fluids 18: 204–206

Weigand A (1993) The response of a vortex ring to a transient, spatial cut. Dissertation University of California San Diego

Weigand A; Gharib M. (1994) On the evolution of laminar vortex rings. Phys Fluids 7

Willert CE; Gharib M (1991) Digital particle image velocimetry. Exp Fluids 10: 181–193

Willert CE; Gharib M (1992) Three-dimensional particle imaging with a single camera. Exp Fluids 12: 353–358